Applied Mechanics and Materials
ISSN: 1662-7482, Vol. 869, pp 20-28
doi:10.4028/www.scientific.net/AMM.869.20

Submitted: 2017-02-13
Revised: 2017-04-30
Accepted: 2017-05-02
Online: 2017-08-30

Modelling the Brittle/Ductile Transition in Super-Fine Finishing of Carbides

BEAUCAMP Anthony[1,a*]

[1]Department of Micro-Engineering, Kyoto University, Japan

[a]beaucamp@me.kyoto-u.ac.jp

Keywords: Ultra-precision, Super-fine finishing, Process mechanism.

Abstract. Materials such as binderless tungsten carbide and silicon carbide have become ubiquitous in the fabrication of high-performance tooling and molding inserts. But while conventional grinding of these hard ceramics has been studied in depth, the theory underlying their super-fine finishing has been less extensively explored. In particular, the boundary in process parameters that delineates the brittle/ductile removal transition remains mostly undocumented. In this paper, we review some super-fine finishing methods for carbide materials, based on both bound and kinetic abrasive processes. The focus is then placed on modelling the interaction between material and abrasives under their respective process conditions, and deriving some useful criteria guiding the brittle/ductile transition.

Introduction

The fundamentals of micro-grinding carbide materials, (1) super abrasive tooling, (2) ultra-precision machinery, and (3) lubricant delivery, have made striding progress in recent years. Sub-nanometer surface roughness is routinely attained on small aspheric and freeform optical apertures, as required in consumer products (i.e. smartphone lenses and screens) or medical applications (i.e. endoscopes). However, the repeating patterns produced by cusping of the grinding wheel moving across spiral or raster paths is still an important issue that affects the performance of the final products (such as light scattering and diffraction). For this reason, super-fine finishing remains a necessary post-processing step for many high-end applications.

Such finishing process should smooth the surface by removing the cyclic patterns, reduce the overall surface roughness and waviness, but avoid generating further sub-surface damage or texturing of the surface that could negatively impact on the lifetime of the tool or mold insert. Deterministic finishing of surfaces down to ultra-precision criteria (shape accuracy of 1 part in 10^9) has steadily become more widely available on automated CNC machinery, thanks to a number of innovations in sub-aperture finishing [1]. A number of sub-aperture finishing processes qualify in all these respects, a non-exhaustive list of which includes:

a) Bound abrasives: processes such as grolishing (a soft tool and pad embedded with abrasives) [2], and shape adaptive grinding (SAG, an elastic tool covered with rigid pellets loaded with abrasives) [3].

b) Loose abrasives: processes such as bonnet polishing (an elastic tool with a soft pad and abrasive slurry) [4], fluid jet polishing (FJP, a pressurized stream of abrasive slurry) [5], magnetic abrasive finishing (MAF, a slurry of abrasives and ferrite particles under a magnetic field) [6], elastic emission machining (a stiff elastic wheel in microscopic contact with the workpiece) [7], and ultra-sonic vibration polishing [8].

c) Non-conventional: processes such as reactive plasma (a chemically reactive gas blown over the surface) [9], and ion beam figuring [10].

A common characteristic of such processes is their time dependent nature, whereby the depth of removal is either a quasi-linear factor of the speed at which the tool transverses the surface, or at least follows a predictable and repeatable evolution as a function of time. To control such processes, the feedrate of the sub-aperture work area is moderated such that the tool goes slower over peaks, and faster over valleys, of the form error profile. The convergence rate of the corrective operation

(ratio of the rms of the form error before/after each correction) usually depends on the accuracy of the measurement system and ability of the machine to deliver the commanded tool path. In this paper, we discuss theoretical modelling aspects in abrasive based super-fine finishing of hard ceramic materials, and extract some useful criteria to delineate the different removal regimes.

Properties of carbide materials

Crack formation in brittle materials. Ceramic materials such as tungsten carbide and silicon carbide offer high thermal stability and specific stiffness, which makes them well suited for high temperature / high pressure applications such as tooling and molding inserts. Understanding the mechanism in fine grinding and polishing of these brittle materials has become an important research topic. Klocke et al [11] compared in details the two main regimes of material removal: brittle and ductile, as shown in Fig. 1. Malkin et al. [12] have shown that pre-machining ceramics in the brittle mode generates sub-surface damage in the form of lateral and median cracks. These cracks are associated with residual stresses (i.e. areas of compressive and tensile stress around the cracks) that impact on the surface integrity of the workpiece (e.g. premature brittle failure of insert molds) [13]. Additionally, their lateral dimension is close to the wavelength of visible light so they can also negatively impact on the optical performance of the final product. Thus, material removal in the final finishing step should be sufficiently deep for these micro-cracks to be eliminated from the reflecting surface. But this usually results in low productivity and high energy use, since removal rate in polishing is orders of magnitude lower than grinding.

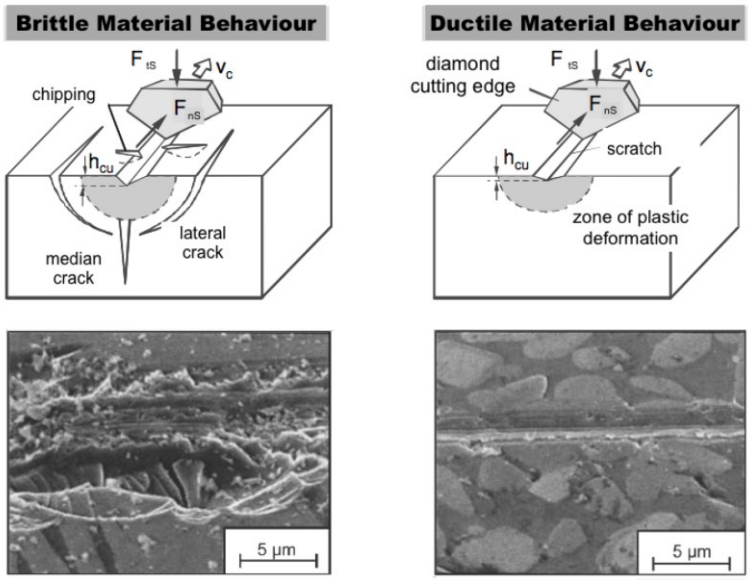

Fig. 1. Comparison of brittle/ductile removal regimes [11].

Brittle-ductile transition. According to Bifano et al. [14], the brittle-ductile transition in ceramic materials relates to a critical depth of indentation d_c. This critical depth can be expressed as a function of measurable material properties as follows:

$$d_c = 0.15 \left(\frac{E}{H}\right) \left(\frac{K_c}{H}\right)^2 \quad (1)$$

where E is the elastic modulus of the material, H the Vickers hardness, and K_c the fracture toughness. The validity of the coefficient 0.15 was verified for several ceramic materials including fused silica, zerodur and silicon carbide [14]. It corresponds to an arbitrary 10 percent fracturing of the indentation walls. Table 1 shows a summary of these material properties for silicon carbide and tungsten carbide [15], together with the resulting value for critical depth of indentation.

Table 1. Material properties of binderless carbides used in optical mold fabrication.

	Silicon carbide	**Tungsten carbide**
Elastic modulus (E)	410 [GPa]	715 [GPa]
Fracture toughness (K_c)	4.6 [MPa.m$^{1/2}$]	4.8 [MPa.m$^{1/2}$]
Vickers hardness (H)	2800 [Kg.mm^{-2}]	2350 [Kg.mm^{-2}]
Critical depth of indentation (d_c)	59 [nm]	190 [nm]

When considering a finishing process, given that the equivalent indentation depth d_i can be expressed as function of process parameters, it is possible to use the critical indentation depth model to predict brittle-ductile transition through the relationship $d_i < d_c$. Bifano verified the validity of this relationship in ceramic material grinding by varying the infeed rate, as shown in fig. 2 where the blue lines indicates the 10% wall fracturing threshold between brittle and ductile regime.

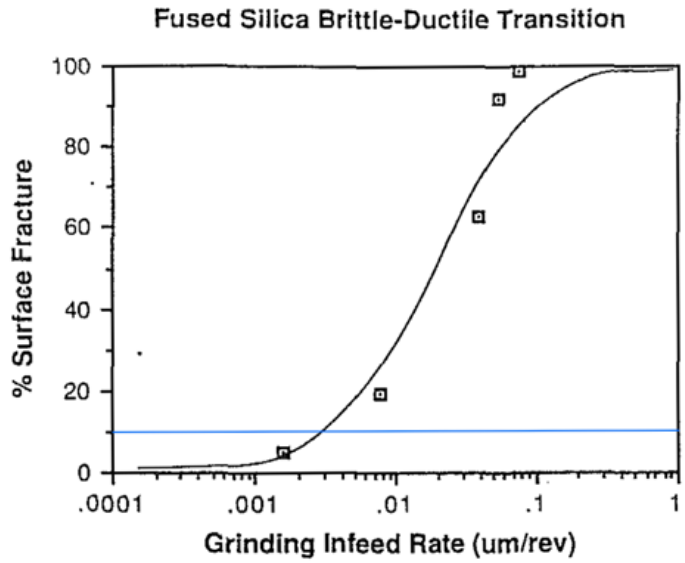

Fig. 2. Brittle-ductile transition observed on fused silica [14].

In the following sections, we consider two types of finishing processes that are applicable to aspherical and freeform shapes: shape adaptive grinding (a bound abrasives process), and fluid jet polishing (a kinetic abrasive process). The mechanisms of these processes are examined in the context of brittle-ductile transition theory.

Shape adaptive grinding (SAG)

Principle of SAG. Shape Adaptive Grinding (SAG) [16-18] was proposed as a process for freeform finishing of difficult materials such as ceramics and high-performance alloys. The basic principle of SAG, shown in fig. 3, can be described as "semi-elasticity": using an elastic spherical tool, overall compliance is achieved with freeform workpieces over a sub-aperture grinding area, while hard contact is simultaneously achieved at relatively smaller scale thanks to rigid pellets covering the elastic tool. Nickel or hard resin pellets are typically used, inside which super-abrasives such as diamond or cubic boron nitride (CBN) are embedded. The size of the grinding area is controlled by offsetting this elastic sphere against the workpiece, while the grinding direction and speed can be controlled independently through the angle of attack and rotation speed of the tool.

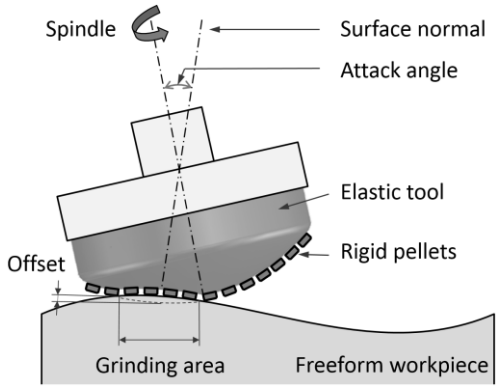

Fig. 3. Principle of Shape Adaptive Grinding (SAG) [16].

Mechanism in SAG. The semi-elasticity of SAG tools allows for the following assumptions to be made when they contact a workpiece:

- Mechanical strain is borne by the elastic support material rather than the rigid pellets.
- Strains are within the elastic limit of this support material.
- The contact area is significantly smaller than the overall size of the support material.

Under these assumptions, when the tool is statically contacting the workpiece surface then the contact pressure *P(r)* can be derived from Hertz theory for contact between a sphere and half-space:

$$P(r) = P_{max}\sqrt{\left(1 - \frac{r^2}{R_t\, O_t}\right)} \tag{2}$$

where r is the radial position in the contact area, R_t the SAG tool radius, O_t the tool offset, and P_{max} is the maximum contact pressure for which the expression is:

$$P_{max} = \frac{2\, E_{eq}\sqrt{O_t}}{\pi\sqrt{R_t}} \tag{3}$$

where E_{eq} is the equivalent elastic modulus of the contact.

The "semi-elasticity" of SAG tools ensures good compliance of the pellets with the work surface. In the case of workpieces with a radius of curvature larger than 25 mm, variation in height across a 0.5 mm pellet is less than 1µm. It may then be assumed that all abrasives within the pellet are contacting the surface. This assumption is corroborated by micrographs of partially worn SAG tools, as shown in fig. 4. In the case of both resin and nickel binder material, after an initial period of self-dressing that takes up-to 30 min, all diamonds on the pellet surface take on a flattened appearance. This is a strong indicator that they are contacting the work surface during processing.

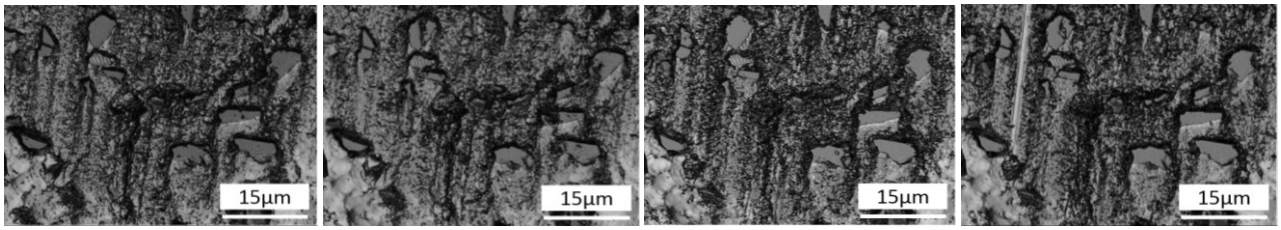

(a) After 30 min (b) After 2.5 hrs (c) After 5 hrs (d) After 10 hrs

Fig. 4. Micrographs of SAG pellet after cumulative grinding time (100x) [17].

By analyzing a large number of micrographs, it is possible to assess the average density of diamond on the pellets. The total number of diamonds in contact with the surface during grinding can then be estimated by integrating across the grinding area. The load on each diamond a_f can thus be estimated by dividing the contact pressure p_r (eq. 2) with the number of diamond per unit of area:

$$a_f = \frac{p_r}{a_n} \tag{4}$$

A schematic of the grinding condition is shown in fig. 5: the rake angle has a small negative value, which implies high loading of the grinding edges. The clearance angle is slightly positive, which allows for debris to flow around the abrasives. Characteristic values of the rake and clearance angles in SAG were previously reported in the literature [17].

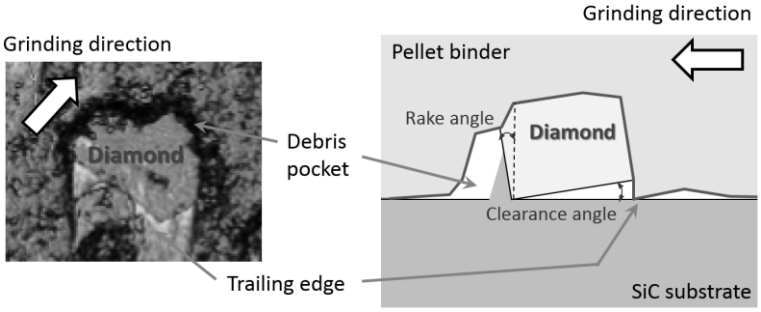

Fig. 5. Close-up of abrasive (left) and diagram of corresponding grinding condition (right) [17].

Based on this observation of the abrasive/workpiece interaction, an expression for the indentation depth of abrasives can be derived that obeys the following rules: (1) it is proportional to the abrasive loading a_f and inversely proportional to the abrasive edge width a_w, (2) inversely proportional to the square root of the material hardness H, (3) weakly affected by the relative velocity of abrasives a_v. This leads to the following expression for the indentation depth d_i, which contains unknown coefficients (α, β, γ) that may be characterized empirically:

$$d_i = \left(\frac{\alpha}{\sqrt{H}}\right)\left(\frac{a_f}{a_w}\right)(1 + \beta {a_v}^{\gamma}) \tag{5}$$

Brittle-ductile transition. Coefficients of the equivalent indentation depth experession were derived experimentally by carrying out single abrasive fly-mill experiments on silicon carbide, and measuring the indentation depth as a function of process parameters including the tool radius, offset and elasticity, as well as the abrasives size and loading [18]. The coefficients were thus determined to be: $\alpha \approx 0.03$, $\beta \approx 0.01$, $\gamma \approx 0.5$.

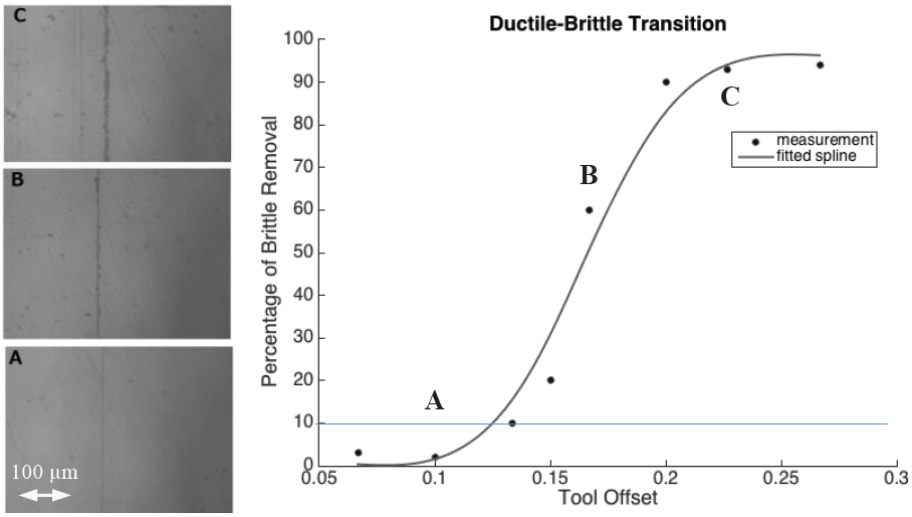

Fig. 6. Brittle-Ductile transition observed in SAG finishing of silicon carbide [18].

Fig. 6 shows the brittle-ductile transition corresponding to the criteria established by Bifano: a selection of micrographs called zones A, B and C are shown on the left side. The percentage of wall fracture was extracted visually, and used to draw the graph on the right hand-side where the blue line indicates the 10% threshold. According to this plot, ductile-brittle transition occurs for tool offset between 0.1 and 0.15 mm. This result was found to be in good agreement with the transition zone predicted by the relationship $d_i < d_c$.

Fluid jet polishing (FJP)

Principle of FJP. In recent years, Fluid Jet Polishing (FJP) has been studied for its potential as a finishing method for small and intricately shaped molding inserts [19,20]. Some advantages of this process include the ability to generate sub-millimeter polishing footprints, a wide range of material removal rates through variation of the abrasive grit size and inlet pressure, a propensity for removing machining marks from prior processes without introducing another tool signature, as well as the absence of tool wear.

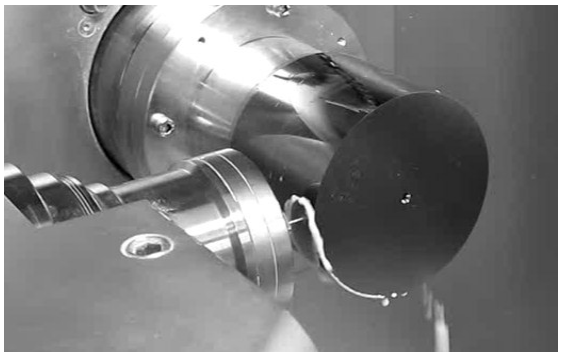

Fig. 7. Fluid jet polishing of mandrel for X-ray mirror replication [19].

In the FJP process, shown in fig. 7, a mixture of water and abrasive particles is delivered by a pump to a converging nozzle of outlet diameter usually between 0.1 and 2.0 mm. The jet impinges the workpiece, thus generating a polishing spot. The typical pressure range for the slurry inlet is between 1 and 20 bar, while abrasive grit size may range from 0.1 to 50 µm. FJP typically delivers a surface finish that is a factor of inlet pressure, material type, abrasive type and grit size.

Mechanism in FJP. Fluid flow in FJP can be characterized using the Navier-Stokes equations, which arise from the application of Newton's second law to viscous fluids. Since fluid jet polishing operates at relatively low pressures, and slurry temperature is stabilized externally, the assumption can be made that fluid density remains mostly constant inside the system. The incompressible form of the Navier-Stokes equations can be used in such case to describe the fluid velocity field:

$$\rho\left(\frac{\partial \mathrm{v}}{\partial \mathrm{t}} + \mathrm{v}.\nabla \mathrm{v}\right) = -\nabla \mathrm{p} + \mu\nabla^2 \mathrm{v} + \mathrm{f} \tag{6}$$

where v (m/s) is the fluid velocity field, p (Pa) the fluid pressure, ρ (kg/m3) the fluid density, μ (Pa.s) the fluid viscosity, and f (N) represents external forces acting on the fluid. After computing the fluid flow, a study of the motion of particles within the slurry can be carried out. For particles with mass m, the trajectory $p(t)$ can be derived from Newton's second law of motion:

$$\mathrm{m}\frac{\partial^2 \mathrm{p}}{\partial \mathrm{t}^2} = \mathrm{F} \tag{7}$$

where m is the particle's mass, and F the sum of forces acting on the particle. The external forces acting on a particle are comprised of gravitation, buoyancy, drag, and collisions with other particles. It is assumed that particle collisions cancel each other out across the entire fluid domain. And because of the high fluid velocity, it is assumed that gravitation, buoyancy, and collisions are all small compared with the drag force. The drag force can be calculated from Rayleigh's equation:

$$\mathrm{F} = \rho \mathrm{C_D} \mathrm{v}^2 \frac{\mathrm{A}}{2} \tag{8}$$

where ρ is the density of the fluid, C_D the drag force coefficient (inversely proportional to the Reynolds number), v the velocity relative to the fluid, and A the projected area of the particle.

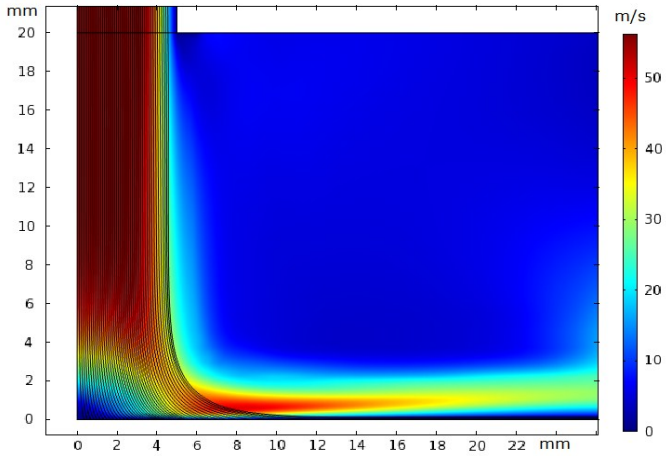

Fig. 8. Fluid velocity (color scale) and Particle tracing (black lines) [19].

Velocities computed from a typical computational fluid dynamics simulation are shown in Fig. 8: slurry exits the nozzle from the upper-left side, and impacts the horizontal workpiece surface at the bottom. The fluid propagates with speeds shown in the color bar. As for simulated particle impacts, shown as black trajectories, an expression for the indentation depth of abrasives can be derived that obeys the following rules: (1) it is proportional to the kinetic energy E_k of abrasives and inversely proportional to their projected area A, (2) inversely proportional to the square root of the material hardness H. This leads to the following expression for the indentation depth d_i, which contains an unknown coefficient (α) that may be characterized empirically:

$$d_i = (\frac{\alpha}{\sqrt{H}})(\frac{E_k}{A}) \tag{9}$$

Brittle-ductile transition. The coefficient of the equivalent indentation depth experession was derived experimentally by carrying out low concentration slurry experiments on tungsten carbide, and measuring the indentation depth as a function of process parameters including the inlet pressure, nozzle size, as well as the abrasives size and density. The coefficient was determined to be close to that found in SAG: $\alpha \approx 0.05$.

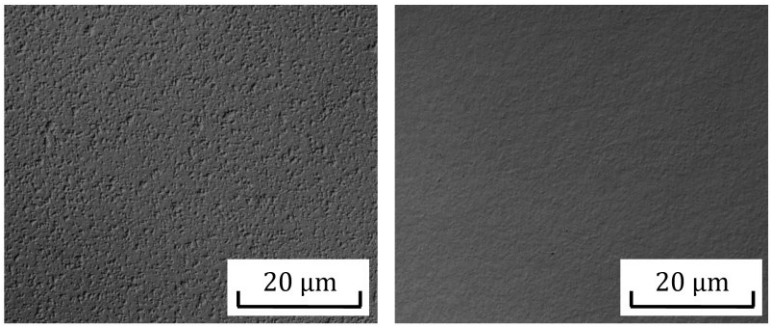

Fig. 9. Brittle-Ductile transition observed in FJP finishing of tungsten carbide [20].

Fig. 9 shows the typical machined surface condition when operating just above (left), and below (right) the brittle-ductile transition, as defined through the criteria established by Bifano. Brittle removal by the kinetic abrasives results in extensive pitting on the surface, whereas ductile removal results in a randomly textured surface with no directional process signature.

Summary

In this paper, an overview was provided of the mechanical properties of ceramic materials used in tooling and mold inserts fabrication, such as silicon carbide and tungsten carbide. Bifano's critical depth of indentation was used as a criteria against which predictive models of the brittle-ductile transition in finishing processes can be derived. The validity of this criteria was shown to

extend at least to two different types of abrasive processes called shape adaptive grinding and fluid jet polishing, which are directly applicable to fine finishing of aspheric and freeform carbide artifacts. Advantages of such a predictive model for the brittle/ductile transition boundary in carbide materials include the ability to maintain process parameters in the ductile regime which leads to higher surface integrity, as well as improving productivity by pushing material removal rate to its highest possible value without causing brittle damage to the workpiece surface.

Acknowledgments

This work was supported by the JSPS Grant-in-Aid for Scientific Research No. 15H06320 from the Japan Society for the Promotion of Science.

References

[1] Evans C., Paul E., Dornfeld D., Lucca D., Byrne G., Tricard M., Klocke F., Dambon O., Material removal mechanisms in lapping and polishing, Annals of the CIRP, 52/2 (2003) 611-633.

[2] Yu G., Walker D., Li H., Implementing a grolishing process in Zeeko IRP machines, Applied optics, 51/27 (2012) 6637-6640.

[3] Beaucamp A., Namba Y., Combrinck H., Charlton P., Freeman R., Shape adaptive grinding of CVD silicon carbide, Annals of the CIRP, 63/1 (2014) 317-320.

[4] Walker D., Beaucamp A., Freeman R., McCavana G., Morton R., Use of the Precessions process for pre-polishing and correcting 2D & 2.5D Form, Optics Express, 14/24 (2006) 11787-11795.

[5] Messelink W., Faehnle O., Exploiting the Process Stability of Fluid Jet Polishing, Optical Fabrication and Testing, OSA Technical Digest (2008) OThD3.

[6] Riveros R., Mitsuishi I., Takagi U., Ezoe Y., Mitsuda K., Yamaguchi H., Boggs T., Ishizu K., Magnetic Field-Assisted Finishing of Silicon Microelectromechanical Systems Micropore X-Ray Optics, Journal of Manufacturing Science and Engineering, 134/5 (2012) 051001.

[7] Mori Y., Yamauchi K., Endo K., Elastic emission machining, Precision Engineering 9/3 (1987) 123-128.

[8] Suzuki H., Moriwaki T., Okino T., 2006, Development of ultrasonic vibration assisted polishing machine for micro aspheric die and mold, Annals of the CIRP, 55/1: 385-388.

[9] Mori Y., Yamauchi K., Yamamura K., Sano Y., Development of plasma chemical vaporization machining, Rev. of Scientific Instruments, 71/12 (2000) 4627-4632.

[10] Drueding T., Fawcett S., Wilson S., Bifano T., Ion beam figuring of small optical components, Optical engineering, 34/12 (1995) 3565-3571.

[11] Klocke F. and König W., Manufacturing Processes 2 (2009).

[12] Malkin S. and Ritter J., Grinding mechanisms and strength degradation for ceramics. Journal of Engineering for Industry 111/2 (1989) 167-174.

[13] D. Magda, Understanding the Effect of Residual Stresses on Surface Integrity and how to Measure them by a Non-Destructive Method. ASEE (2008) 13.1313.1-17

[14] T. Bifano, T. Dow, R. Scattergood, Ductile-regime grinding: a new technology for machining brittle materials. Transactions of ASME 113 (1991) 184-189.

[15] H. Kim, J. Kim, Y. Kwon, Mechanical properties of binderless tungsten carbide by spark plasma sintering. Proc. 9th Russian-Korean International Symposium on Science and Technology (2005) 458-461.

[16] A. Beaucamp, Y. Namba, H. Combrinck, P. Charlton, R. Freeman, Shape adaptive grinding of CVD silicon carbide. Annals of the CIRP 63/1 (2014) 317-320.

[17] A. Beaucamp, Y. Namba, P. Charlton, Process mechanism in shape adaptive grinding (SAG). Annals of the CIRP 64/1 (2015) 305-308.

[18] A. Beaucamp, P. Simon, P. Charlton, C. King, A. Matsubara, K. Wegener, Brittle-ductile transition in shape adaptive grinding (SAG) of SiC aspheric optics. International Journal of Machine Tools and Manufacture (2016).

[19] A. Beaucamp, Y. Namba, R. Freeman, Dynamic Multiphase Modeling and Optimization of Fluid Jet Polishing Process. Annals of the CIRP 61/1 (2012) 315-318.

[20] A. Beaucamp, Y. Namba, W. Messelink, D. Walker, P. Charlton, R. Freeman, Surface integrity of fluid jet polished tungsten carbide. Procedia CIRP 13 (2014) 377-381.